



G.W.C. Whiting
School of Engineering

AFOSR-TR- 89-0086

2

The Johns Hopkins University

DTIC FILE COPY

AD-A205 196

A FUNDAMENTAL UNDERSTANDING OF THE EFFECT OF ALLOYING ELEMENTS ON THE CORROSION RESISTANCE OF RAPIDLY SOLIDIFIED Mg ALLOYS

FINAL REPORT

DTIC
ELECTE
FEB 16 1989
S D

DISTRIBUTION STATEMENT A
Approved for public release
Distribution Unlimited

J. Kruger, G.L. Makar, G.G. Long,
D.K. Tanaka and A. Joshi
December 23, 1988

F496620-86-C-0014, P00002
AIR FORCE OFFICE OF
SCIENTIFIC RESEARCH

89 2 15 167

REPORT DOCUMENTATION PAGE

Form Approved
OMB No. 0704-0188

1a. REPORT SECURITY CLASSIFICATION Unclassified	1b. RESTRICTIVE MARKINGS N.A.
2a. SECURITY CLASSIFICATION AUTHORITY	3. DISTRIBUTION / AVAILABILITY OF REPORT Unlimited
2b. DECLASSIFICATION / DOWNGRADING SCHEDULE	

4. PERFORMING ORGANIZATION REPORT NUMBER(S) F496620-86-C-0014, P00002	5. MONITORING ORGANIZATION REPORT NUMBER(S) AFOSR-TR-89-0086
--	---

6a. NAME OF PERFORMING ORGANIZATION Johns Hopkins University	6b. OFFICE SYMBOL (if applicable)	7a. NAME OF MONITORING ORGANIZATION Air Force Office of Scientific Research
---	-----------------------------------	--

6c. ADDRESS (City, State, and ZIP Code) 102 Maryland Hall Baltimore, MD 21216	7b. ADDRESS (City, State, and ZIP Code) AFOSR Bldg. 410-NE Bolling AFB, DC 20332
---	---

8a. NAME OF FUNDING / SPONSORING ORGANIZATION AFOSR	8b. OFFICE SYMBOL (if applicable) NE	9. PROCUREMENT INSTRUMENT IDENTIFICATION NUMBER F49620-86-C-0014
--	---	---

8c. ADDRESS (City, State, and ZIP Code) Bldg. 410-NE Bolling AFB, DC 20332	10. SOURCE OF FUNDING NUMBERS		
	PROGRAM ELEMENT NO. 101102F	PROJECT NO. 2300	TASK NO. A1

11. TITLE (Include Security Classification)
A Fundamental Understanding of the Effect of Alloying Elements on the Corrosion Resistance of Rapidly Solidified Mg Alloys

12. PERSONAL AUTHOR(S) J. Kruger, G.G. Long, G.L. Makar, D.K. Tanaka and A. Joshi

13a. TYPE OF REPORT Final	13b. TIME COVERED FROM 11/1/85 to 10/31/88	14. DATE OF REPORT (Year, Month, Day) 88-12-23	15. PAGE COUNT 37
------------------------------	---	---	----------------------

16. SUPPLEMENTARY NOTATION

17. COSATI CODES	18. SUBJECT TERMS (Continue on reverse if necessary and identify by block number) Mg alloys, rapidly solidified alloys, corrosion, EXAFS, electrochemistry, localized corrosion, passivity. (GFS)											
<table border="1"> <thead> <tr> <th>FIELD</th> <th>GROUP</th> <th>SUB-GROUP</th> </tr> </thead> <tbody> <tr><td> </td><td> </td><td> </td></tr> <tr><td> </td><td> </td><td> </td></tr> <tr><td> </td><td> </td><td> </td></tr> </tbody> </table>		FIELD	GROUP	SUB-GROUP								
FIELD	GROUP	SUB-GROUP										

19. ABSTRACT (Continue on reverse if necessary and identify by block number)

This third and final report describes progress made in the following areas concerned with the effect of alloying elements on the corrosion resistance of RSP Mg alloys: 1) A new x-ray absorption technique (reEXAFS) was developed that found that the more corrosion resistant an alloy was, the higher the Mg(OH)₂ content and the less crystalline were the films on its surface, as predicted from theoretical considerations developed in the first year, 2) Electrochemical studies were carried out on the effect of Al, Zn, C, Nd, Y, Mn, Ii and Ca in melt-spun Mg ribbons and an extruded alloy made from crushed RSP ribbons on corrosion behavior. The corrosion rate decreased with increased percentages of Al and small additions of Zn. It was found that rapid solidification improves the resistance of the alloy studied (AZ61) to localized Cl⁻ attack; 3) Surface analytical studies found that only Li and Ca have a tendency to be enriched in the films on RSP alloys. Hydroxides and carbonates were found in the surface films along with oxides, 4) Studies of the rates of repassivation, a factor important in stress corrosion susceptibility, was found to not differ greatly between a cast and an RSP alloy.

20. DISTRIBUTION / AVAILABILITY OF ABSTRACT <input type="checkbox"/> UNCLASSIFIED/UNLIMITED <input type="checkbox"/> SAME AS RPT. <input type="checkbox"/> DTIC USERS	21. ABSTRACT SECURITY CLASSIFICATION Unclassified
--	--

22a. NAME OF RESPONSIBLE INDIVIDUAL M. Kruger	22b. TELEPHONE (Include Area Code) (301) 283-8937	22c. OFFICE SYMBOL NE
--	--	--------------------------

**A FUNDAMENTAL UNDERSTANDING OF THE EFFECT OF ALLOYING
ELEMENTS ON THE CORROSION RESISTANCE OF RAPIDLY SOLIDIFIED
Mg ALLOYS**

J. Kruger, G.L. Makar, G.G. Long, D.K. Tanaka and A. Joshi

ABSTRACT

This third and final report describes progress made in the following areas concerned with the effect of alloying elements on the corrosion resistance of RSP Mg alloys:

- 1) A new x-ray absorption technique (reflEXAFS) was developed that found that the more corrosion resistant an alloy was, the higher the $Mg(OH)_2$ content and the less crystalline were the films on its surface, as predicted from theoretical considerations developed in the first year.
- 2) Electrochemical studies were carried out on the effect of Al, Zn, Ce, Nd, Y, Mn, Li and Ca in melt-spun Mg ribbons and an extruded alloy made from crushed RSP ribbons on corrosion behavior. The corrosion rate decreased with increased percentages of Al and small additions of Zn. It was found that rapid solidification improves the resistance of the alloy studied (AZ61) to localized Cl^- attack.
- 3) Surface analytical studies found that only Li and Ca have a tendency to be enriched in the films on RSP alloys. Hydroxides and carbonates were found in the surface films along with oxides.
- 4) Studies found that the rates of repassivation, a factor important in stress corrosion cracking susceptibility, did not differ greatly between a cast and an RSP alloy.



Accession For	
NTIS CRA&I	<input checked="" type="checkbox"/>
DTIC TAB	<input type="checkbox"/>
Unannounced	<input type="checkbox"/>
Justification	
By _____	
Distribution/	
Availability Codes	
Dist	Avail and/or Special
A-1	

INTRODUCTION

This Third Annual and Final Report describes the progress achieved in the past three years. The report is divided into five sections as follows:

Section I Theoretical studies were carried out during the first year that examined how alloying constituents affect the corrosion resistant properties of surface films on RSP Mg alloys and the development of a list of the most promising constituents to study.

Section II The application of electrochemical techniques to study the corrosion behavior of the Mg alloys chosen were completed. This aspect has resulted in one paper accepted for publication and one paper to be submitted in January 1989.

Section III A new x-ray absorption technique especially adapted to the study of thin surface films, reEXAFS, was developed. This new technique was applied to the study of cast and RSP Mg alloys that were found to be more corrosion resistant. This part of the work has resulted in one paper accepted for publication and four papers to be submitted in early 1989.

Section IV This describes surface analytical studies carried out by Lockheed, a sub-contractor for the first two years of this contract.

Section V New studies initiated during the third year concerned with the stress corrosion cracking susceptibility of RSP Mg alloys is described in this section.

SECTION I

Theoretical Studies

Dr. Akos Revesz was employed as a consultant on this project to examine to role of alloying constituents on film properties and to carry out theoretical studies what would suggest alloying constituents that show the most promise for the development of RSP alloys with improved corrosion resistance. Working with Lockheed Palo Alto Research Laboratory which is a subcontractor on this project, he helped develop a list of binary RSP alloys (Table 1) that were selected for study by this project as well as for the complimentary AFWAL project (on which Johns Hopkins was a subcontractor in the first and second years of this project).

Table 1 - Binary Alloys Proposed for Study

Mg-5%Si	Mg-10%Zn
Mg-15%Al	Mg-20%Zn
Mg-30%Al	Mg-30%Zn
Mg-45%Al	Mg-2%Li
Mg-1%Mn	Mg-8%Li
Mg-5%Mn	Mg-14%Li
Mg-5%Ca	Mg-1%P
Mg-15%Ca	Mg-1%Cr
Mg-45%Ca	

The majority of these alloys were supplied by Lockheed to Johns Hopkins for this study and the complimentary AFWAL project.

In addition to the development of a list of binary alloys for experimentation, a study was carried out to examine the factors affecting the protective nature of the films that form on Mg alloys. The following points were developed:

1. The ratio of molar volumes of the oxide (hydroxide) and the metal affects the protective nature of the film (Pilling-Bedworth Rule), the ratio being 0.85 for MgO (unprotective) and 1.88 for Mg(OH)₂ (protective).
2. Films with glassy (vitreous) structures provide superior corrosion protection (1). Factors that promote more protective films are those that increase the flexibility of the structure of an oxide or hydroxide film. With regard to

MgO or Mg(OH)₂ the following can be proposed:

a) Since hydrogen bonding increases structural flexibility introducing Al, Zn or B, all of whose hydroxides possess hydrogen bonding, into a magnesium alloy could promote hydrogen bonding in Mg(OH)₂ which does not contain hydrogen bonds(2).

b) Silicon additions to Mg can diffuse along grain boundaries to the Mg surface where it forms a vitreous protective SiO₂ layer (3).

SECTION II

Alloy Composition and Corrosion Behavior

This work focused on using electrochemical techniques to determine the effect of various alloying elements and their concentration on the corrosion rates of binary RS Mg alloys produced by melt-spinning. This processing route was selected because of the chemical and microstructural homogeneity which these ribbons tend to possess. The ribbons are small and fragile, however, and they are therefore not suitable for evaluation using the traditional weight-loss techniques, such as immersion or salt-spray tests. Electrochemical impedance spectroscopy (EIS) was therefore selected to evaluate the alloys, and a significant objective of this work was to establish a correlation between the corrosion rates calculated using electrochemical techniques and those calculated from weight loss of bulk specimens. Also reported here are the results of anodic polarization scans used to compare the protective ability of the passive films formed on alloy AZ61 (Mg-6Al-1Zn) in the cast and melt-spun condition. Finally, scanning electron microscopy (SEM) provided additional insights into the corrosion processes occurring on several cast and RS alloys. Table I lists the binary RS alloys examined, with compositions given in weight percent. Three types of electrochemical experiments were conducted: electrochemical impedance spectroscopy, linear polarization near the corrosion potential (E_{oc} or E_{corr}), and potentiodynamic anodic polarization. Gravimetric studies were also carried out to establish the accuracy of electrochemical corrosion-rate measurements.

Table I. RS Binary Alloys Examined in This Study.

ALLOYING ELEMENT				
Aluminum	Zinc	Lithium	Calcium	Silicon
Mg-14.4Al	Mg-4.8Zn	Mg-2.0Li	Mg-5.5Ca	Mg-1.7Si
Mg-28.8Al	Mg-18.6Zn	Mg-7.7Li	Mg-11.3Ca	
Mg-42.8Al	Mg-27.5Zn	Mg-14.0Li		

*Compositions are given in weight percent.

Results and Discussion

Correlating EIS and Gravimetric Corrosion-Rate Measurements - The goal of the weight-loss studies discussed here was to evaluate how successfully EIS was used to determine the polarization resistance (R_p), a parameter that enables the calculation of the corrosion rates of the magnesium alloys. Five magnesium-base materials in bulk form were examined in these experiments: high-purity magnesium, commercial alloy AZ61, high-purity Mg-30Al, an Mg-Al-Zn-Y alloy, and an Mg-Al-Zn-Nd alloy (the last two were kindly provided by Dr. C.F. Chang of Allied-Signal Corp). These materials were all in the as-cast form, except for the Mg-Al-Zn-Nd alloy, which was extruded from crushed RS ribbon into bar form. Electrochemical impedance spectra, in both Nyquist and Bode formats [1], are shown for pure Mg, cast AZ61, and cast Mg-Al-Zn-Y in Figures 1-3. Figures 1 and 3 are representative of the impedance data for some of the alloys examined in this study, showing a single capacitive semicircle indicative of a charge-transfer process only. Note, however, that the low-frequency data for cast AZ61 (Figure 2) shows an additional time constant, the origin of which has not yet been identified. It appeared in the alloys high in aluminum, and was generally absent in those alloys having less than about 5% Al. This low-frequency behavior resembled a charge-transfer impedance in some cases and a diffusion impedance in others. The impedance of these Al-containing alloys at low frequency may be related to the role of the surface film, which would be expected to gain significance as Al content increases.

Since the Randles circuit model used to analyze the data does not apply to alloys with this additional time constant, a new approach was necessary for determining the corrosion rate based on the complex impedance behavior described above. In cases where corrosion is not controlled by one-step, Tafel behavior, charge-transfer reactions, the polarization resistance (the slope of the steady-state polarization curve at E_{oc}) may no longer serve as a measure of the corrosion rate. In many such cases (eg. diffusion control, multistep electron transfer), it is the charge-transfer resistance (R_{ct}) which may be used in a Stern-Geary [2] expression to determine the corrosion rate [3]. With respect to the frequency spectrum of AZ61 (Figure 2), R_{ct} corresponds to the diameter of the high-frequency capacitive semicircle. Therefore, all corrosion rates determined using EIS in this study were based on the diameter of the high-frequency capacitive semicircle. This corresponds to R_{ct} in all cases, and to R_p in those cases where the impedance spectrum collapses to RC-R behavior ($R_{ct}=R_p$). Figure 4 compares the corrosion rates measured in 0.05M Na borate (pH 9.2) using EIS, linear polarization, and gravimetric analysis.

These results indicate that impedance spectroscopy measured the uniform corrosion rates of these materials relatively accurately, except for the pure magnesium, which had a weight loss roughly an order of magnitude higher than that predicted by EIS or linear polarization.

This failure of the electrochemical results to agree with gravimetric results for pure Mg may be attributed to a "negative difference" effect which relates the observed corrosion rate upon application of an external current to the corrosion rate in the absence of external current [4]. The following equation describes the theoretical relationship between these quantities:

$$I_{corr} + I_{app} - I_{obs} = 0 \quad (1)$$

where:

I_{corr} = the corrosion rate at open circuit

I_{app} = the current applied to hold the specimen at some potential not equal to E_{oc}

I_{obs} = the observed corrosion rate when I_{app} is applied

Marsh and Schaschl [4] found that for steel these components could sum to a number greater than zero (positive difference) or less than zero (negative difference). In this work, equation 5 reduces to a difference between I_{corr} and I_{obs} , since the experiments were conducted under open-circuit conditions ($I_{app}=0$). Since the weight loss (I_{obs}) was higher than the dissolution rate determined using electrochemical techniques (I_{corr}), Figure 4 indicates a negative difference for pure Mg. This phenomenon has been reported for magnesium dissolution in several previous studies [5,6,7,8].

Petty et al. attributed the discrepancy to the existence of univalent magnesium [6]. This changes the corrosion rate calculated from electrochemical data because it changes the average valence used to convert corrosion current (i.e. charge passed) to a penetration rate. Another theory for the origin of the discrepancy was advanced by Straumanis and Bhatia, who studied the anodic dissolution of magnesium in neutral and acid solutions [7] and James et al. studied the dissolution of Mg in acids [8]. In both cases, the authors attributed much of the negative difference to disintegration of the metal into fine particles, describing it as a "chunk" effect. In the present study, scanning electron microscopy (SEM) was used to check for evidence of this phenomenon.

Corrosion of the pure magnesium in sodium borate solution was non-uniform, having an etched appearance when viewed with the naked eye or at low magnification with an optical microscope. This effect was observed after only 1-2 hours in the borate solution and was severe after one week. Electron microscopy allowed a closer inspection of this attack, as seen in the photomicrograph of Figure 5. In contrast, the surface of cast AZ61 is shown in Figure 6 and RS AZ61 in Figure 7 after exposure to 0.05M Na borate. This relatively uniform attack is representative of the materials whose corrosion rates were accurately measured using EIS (Figure 4). Higher magnification was used to determine if undermining of small particles contributed to the non-uniform attack characteristic of the pure magnesium. Figure 8 is an SEM photomicrograph showing a pure Mg surface after a 7-day immersion in pH 9.2 sodium borate followed by removal of the corrosion products. Visible in this photomicrograph is a particle, roughly 15 μm in diameter, which has been partially undermined by dissolution of the surrounding matrix. Such particles were distributed over the surface of all of the pure Mg samples examined, whether or not Cl^- had been present during the immersion.

As stated earlier, the RS ribbons were too thin to permit meaningful gravimetric corrosion rate measurements. Although this precludes a direct evaluation of the accuracy of the electrochemical techniques for measuring the corrosion rates of the ribbons, SEM studies showed that the ribbons were, in general, attacked even more uniformly than the bulk alloys. Based on the bulk alloy studies discussed above, the uniform attack of the ribbon alloys, for example the RS AZ61 shown in Figure 7, implies that the corrosion rates of the RS ribbons were accurately determined using EIS. This is a useful finding because such a correlation has not been previously reported for Mg-base materials. This correlation might be strengthened by determining how representative the electrochemical data are of steady-state conditions. Since the ribbon samples used in the electrochemical studies were immersed for only a few hours, the time dependence of weight loss and the electrochemically determined R_p should be examined in future studies. R_p vs. time behavior, examined for cast Mg in sodium borate/3.5% NaCl using EIS, indicated a decrease in R_p of about 25% in the first 5 days, but little change afterwards. However, rather than an increase in the corrosion rate, this decrease in R_p may be caused mostly by an increase in surface area resulting from the non-uniform attack of pure Mg discussed earlier.

The time dependence of the corrosion rate of a bulk RS Mg-Al-Zn-Nd alloy obtained from Allied-Signal Corp. was also examined. A sample was immersed for two weeks in unbuffered 3% NaCl while generating electrochemical impedance spectra periodically. The goal of these experiments was to use R_{ct} to determine a corrosion rate for comparison with that reported for this alloy by Chang and co-workers from weight loss measurements [9]. One of these impedance spectra is presented in the Nyquist format in Figure 9 with the approximate charge-transfer and polarization resistances labeled. This diagram shows inductive behavior at low frequency, and is similar to the spectrum observed by Epelboin et al. for iron dissolving in sulfuric acid [3]. They observed two inductances, which they attributed to the potential dependence of the surface coverage of hydrogen at lower frequencies and of the anodic intermediate species (FeOH) at higher frequencies. Their weight loss measurements correlated well with R_{ct} . The corrosion rate of the Mg-Al-Zn-Nd alloy determined after several days from R_{ct} compared well with the weight loss value reported by Das and Chang of about 11 mpy. Like the other alloys, this material was attacked uniformly, and R_{ct} changes indicated a decrease in the corrosion rate with time. The corrosion rate measured on the first day was about 20 mpy. This decrease was probably due to an increase in pH at the electrode surface toward a value where thermodynamics predicts that a stable oxide or hydroxide film forms on Mg.

Corrosion Rates of Binary RS Alloys - Figure 10 summarizes the corrosion rates of the binary RS alloys (Table I), measured in pH 9.2 sodium borate using EIS. Reproducibility, as measured by standard deviation, varied widely. Standard deviations ranged from about 3% for Mg-15Al to about 40% for Mg-10Zn. Aluminum is the only element which improved the corrosion resistance, causing the rate to decrease as Al content increased. Surface analyses conducted at the Lockheed Palo Alto Research Laboratory indicated that the air-formed oxide on the Mg-Al alloys was a layered structure composed of MgO/Mg-Al-oxide/substrate, with the oxide (Mg-rich) thinner with increasing Al content [10]. It is likely that this benefit of aluminum is related to the nature of this oxide, the strong tendency for Al to form a stable passive film in this electrolyte, and the lack of galvanic action between Mg and Al in these alloys. These results also show that small additions of lithium do not seriously degrade the corrosion resistance of pure magnesium. Lithium was examined mainly because it has a low density and can form a new BCC

phase. Small amounts of Li added to magnesium caused only a slight increase in the corrosion rate compared to Zn, Ca, and Si, suggesting that lithium additions of about 2 wt.% are tolerable.

Zinc had a somewhat anomalous effect on the corrosion behavior of Mg, as evidenced by the peak seen in Figure 10 at the 18.6 wt.% level. This intermediate addition caused a drastic increase in the corrosion rate, while additions of 4.8% and 27.5% had corrosion rates only slightly higher than that measured for pure Mg. Surface analysis indicated the presence of oxide films whose thickness decreased with increasing Zn content [10]. More recent analysis found that the oxides on the Mg-Zn alloys were magnesium-rich, containing little or no zinc [11]. The 27.5% Zn content is lower than that required for glass formation (42-65 wt.% Zn), so the role of zinc at high levels is unclear and warrants further study. For alloys of practical interest to this study, the Zn content must be small due to its high density, and these corrosion data suggest that low zinc levels are not as harmful as similar levels of silicon and calcium.

Calcium appears to have an effect similar to zinc, causing the corrosion rate to increase up to a maximum, and then decrease with further additions. This raises the question of whether Mg-Ca alloys with calcium contents higher than the 11 wt.% maximum studied here have corrosion rates lower than pure Mg. While weight considerations make high zinc concentrations undesirable, calcium has a density of approximately 1.5 g/cm³, and may therefore be added liberally without sacrificing low density. Additional studies of these alloys seem necessary to determine the causes of the maxima in the corrosion rate curves for Ca and Zn, and to further investigate the Mg-Si and Mg-Li systems for evidence of this effect. Note, however, that alloys high in calcium and silicon are unsuitable for structural applications due to their poor strength and/or ductility. Magnesium alloys high in lithium may have greater applicability and are the subject of a current study by the Aluminum Company of America [12].

Passivity and Breakdown of Alloy AZ61 - The effect of RSP on alloy AZ61 (Mg-6Al-1Zn) was examined using anodic polarization scans in the presence of chloride. The electrolytes used were 0.05M Na borate (pH 9.2) and 0.025M Na carbonate/0.025M Na bicarbonate (pH 10.0) with 100 ppm, 1000 ppm, or 3.5% NaCl. Figure 11 presents anodic polarization data for cast and RS AZ61 ribbon in

the carbonate buffer with 100 ppm NaCl. The characteristic parameters i_p and E_b are indicated. The passive current density, i_p , is an indication of the protective film's ability to maintain a low corrosion rate in the passive regime. The breakdown potential, E_b , is one measure of a metal's resistance to attack by an aggressive species; a higher (more positive) value of E_b indicates better resistance. E_b is a parameter which is dependent on experimental conditions, but is generally considered the potential at which the current begins to rise above its passive value due to breakdown of the film and subsequent pit propagation. Previous studies revealed that i_p and open-circuit dissolution rate were affected little by RSP [13]. However, some interesting improvements are seen in resistance to attack by Cl^- .

Figure 11 shows that the breakdown potential for the RS AZ61 is about 200 mV higher than that for the cast material. This 200 mV improvement was observed in the carbonate buffer at all Cl^- levels. Figure 12 presents the results of similar experiments conducted in the borate buffer with 100 ppm NaCl. The breakdown potentials do not indicate any improvement for the RS material, which was the case for all chloride levels. However, the current increase in the region marked "x" of the curve for the cast material at about -1.5 V (Figure 12) indicates pit initiation. These pits were also observed visually, and hydrogen evolved from them at a low rate during the remainder of the experiment. This event was not accompanied by a sharp current increase which normally occurs when the breakdown potential is exceeded, probably due to the fact that the current involved in the slow propagation of these pits is not large compared to i_p . The implication is that the borate-formed film more readily nucleates pits and is probably less stable on the cast AZ61. Figure 12 shows that the melt-spun alloy began pitting and the cast alloy developed new pits at about 400 mV, this value being slightly higher for the cast material.

These improvements may result from increased homogeneity or the formation of glassy films, possibly a combination of both. Similar results were found by Bertocci and Kruger, who used an electrochemical noise technique to examine the passive films on Fe-Cr-Ni alloys [14]. They showed that the film on a glassy alloy was more resistant to breakdown/repassivation events than that on its crystalline counterpart, but little change in overall current density was observed. Hagans recently studied $\text{Mg}_{70}\text{Zn}_{30}$ metallic glass and pure Mg in a pH 9.3 boric/borate buffer with 1000 ppm Cl^- [15]. The metallic glass formed a more protective film than the pure metal, as reflected in a 400 mV improvement in the breakdown potential and a lower passive current density.

List of Figures

- Figure 1 - Electrochemical impedance data for as-cast pure magnesium in pH 9.2 sodium borate presented in the Nyquist format (top) and Bode magnitude format (bottom).
- Figure 2 - Electrochemical impedance data for as-cast alloy AZ61 (Mg-6Al-1Zn) in pH 9.2 sodium borate presented in the Nyquist format (top) and Bode magnitude format (bottom).
- Figure 3 - Electrochemical impedance data for as-cast Mg-Al-Zn-Y in pH 9.2 sodium borate presented in the Nyquist format (top) and Bode magnitude format (bottom).
- Figure 4 - Comparison of corrosion rates of bulk alloys in pH 9.2 sodium borate determined from electrochemical and gravimetric techniques.
- Figure 5 - SEM photomicrograph of pure magnesium surface after one-week immersion in pH 9.2 sodium borate and subsequent removal of corrosion products.
- Figure 6 - SEM photomicrograph of as-cast AZ61 surface after one-week immersion in pH 9.2 sodium borate and subsequent removal of corrosion products.
- Figure 7 - SEM photomicrograph of RS AZ61 surface after several hours in pH 9.2 sodium borate and subsequent removal of corrosion products.
- Figure 8 - SEM photomicrograph of pure magnesium surface after one-week immersion in pH 9.2 sodium borate and subsequent removal of corrosion products. Shown is a particle, roughly 15 μm in diameter, which has been partially undermined by dissolution of the surrounding matrix.
- Figure 9 - Nyquist plot of electrochemical impedance data for RS Mg-Al-Zn-Nd (extruded) after 14 days in unbuffered 3% sodium chloride showing inductive behavior at low frequency.
- Figure 10 - Corrosion rates of binary RS magnesium alloys determined using EIS.
- Figure 11 - Anodic polarization scans for cast and RS AZ61 in pH 10.0 sodium carbonate/sodium bicarbonate with 100 ppm NaCl.
- Figure 12 - Anodic polarization scans for cast and RS AZ61 in pH 9.2 sodium borate with 100 ppm NaCl.

References

1. D.C. Silverman, "Primer on the AC Impedance Technique," in Electrochemical Techniques for Corrosion Engineering, R. Baboian, ed. (Houston, TX: National Association of Corrosion Engineers, 1986), 73-79.
2. M. Stern and A.L. Geary, "Electrochemical Polarization," Journal of the Electrochemical Society, 104 (1) (1957), 56-63.
3. I. Epelboin, C. Gabrielli, M. Keddam, and H. Takenouti, "Alternating-Current Impedance Measurements Applied to Corrosion-Rate Determination," in Electrochemical Corrosion Testing, ASTM 727, F. Mansfeld and U. Bertocci, eds. (Philadelphia, PA: ASTM, 1981), 150-166.
4. G.A. Marsh and E. Schaschl, "The Difference Effect and the Chunk Effect," This Journal, 107 (12) (1960), 960-965.
5. G.R. Hoey and M. Cohen, "Corrosion of Anodically and Cathodically Polarized Magnesium in Aqueous Media," Journal of the Electrochemical Society, 105 (5) (1958), 245-250.
6. R.L. Petty, W. Davidson, and J. Kleinberg, "The Anodic Oxidation of Magnesium Metal: Evidence for the Existence of Unipositive Magnesium," Journal of the American Chemical Society, 76 (1954), 363-366.
7. M.E. Straumanis and B.K. Bhatia, "Disintegration of Magnesium While Dissolving Anodically in Neutral and Acidic Solutions," This Journal, 110 (5) (1963), 357-360.
8. W.J. James, M.E. Straumanis, B.K. Bhatia, and J.W. Johnson, "The Difference Effect on Magnesium Dissolving in Acids," This Journal, 110 (11) (1963), 1117-1120.
9. C.F. Chang, S.K. Das, D. Raybould, and A. Brown, "Corrosion Resistant High Strength Magnesium Alloys by RSP," Metal Powder Report, 41 (4) (1986), 302-308.
10. A. Joshi, "Rapidly Solidified Magnesium Alloys," Interim Technical Report to the Air Force Wright Aeronautical Laboratories, Lockheed Palo Alto Research Laboratory, January 1987.
11. J. Kruger, G.G. Long, D.K. Tanaka, A. Joshi, and G.L. Makar, "A Fundamental Understanding of the Effect of Alloying Elements on the Corrosion Resistance of Rapidly Solidified Magnesium Alloys," Report to the Air Force Office of Scientific Research, The Johns Hopkins University, November 1987.
12. R.K. Weiss, "A Study of Mg-Li Alloys with Two Phase (HCP+BCC) Structures," Proceedings of the 1988 TMS-AIME symposium entitled Advances in Magnesium Alloys and Composites (Warrendale, PA: TMS-AIME, in print).

13. J. Kruger, G.G. Long, and D.K. Tanaka, "Fundamental Understanding of the Effect of Alloying Elements on the Corrosion Resistance of Rapidly Solidified Magnesium Alloys," Report to AFOSR, The Johns Hopkins University, November 1986.
14. U. Bertocci and J. Kruger, "Studies of Passive Film Breakdown by Detection and Analysis of Electrochemical Noise," Surface Science, 101 (1980), 608-618.
15. P.L. Hagans, "Electrochemical Study of the Passivation and Passive Film Breakdown of $Mg_{70}Zn_{30}$ Metallic Glass," Materials Research Society Symposium Proceedings, 80 (1987), 113-120.

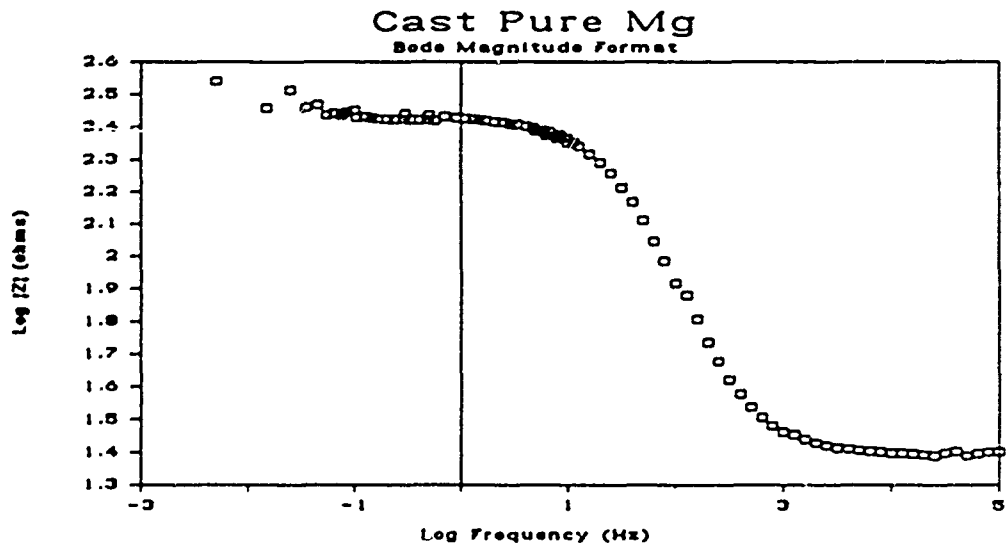
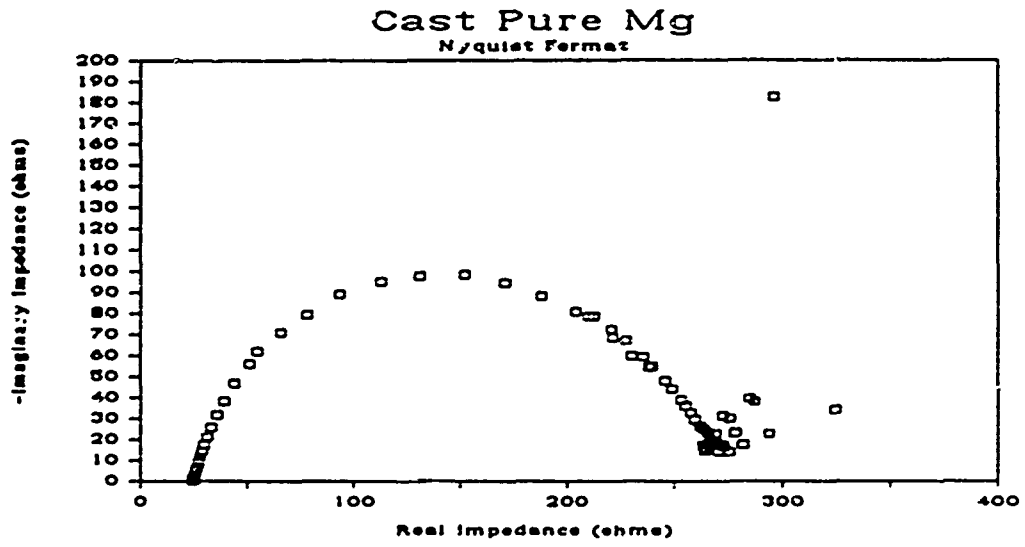


Figure 1

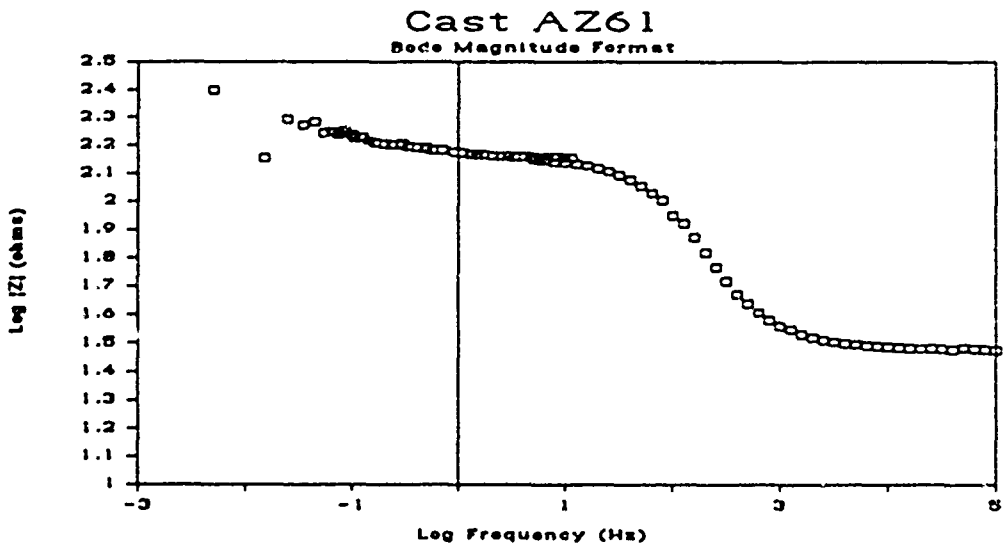
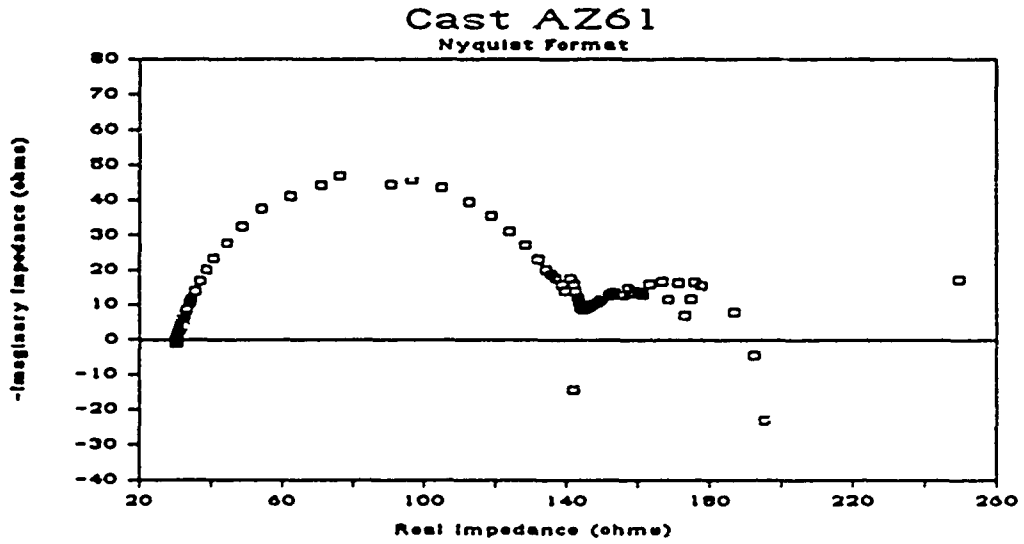


Figure 2

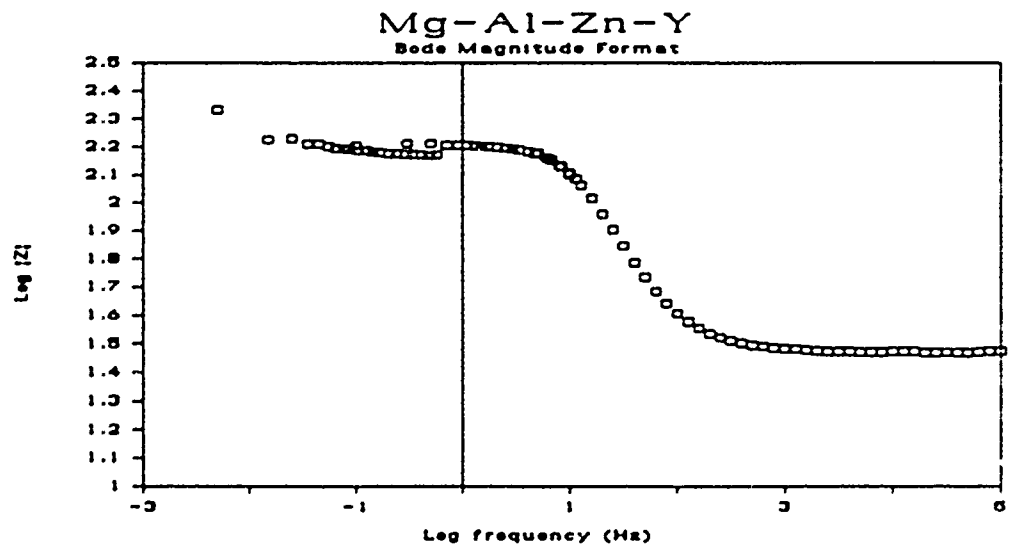
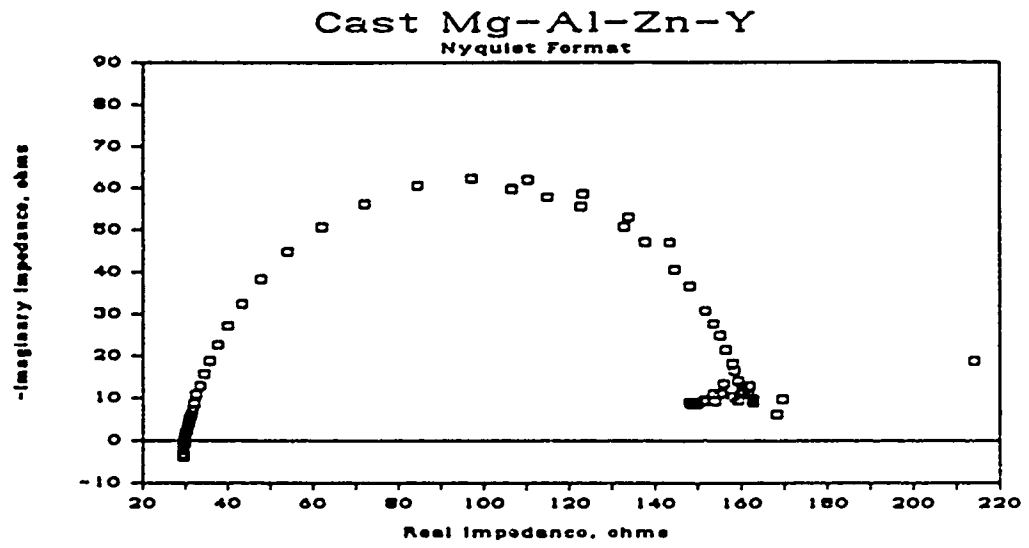


Figure 3

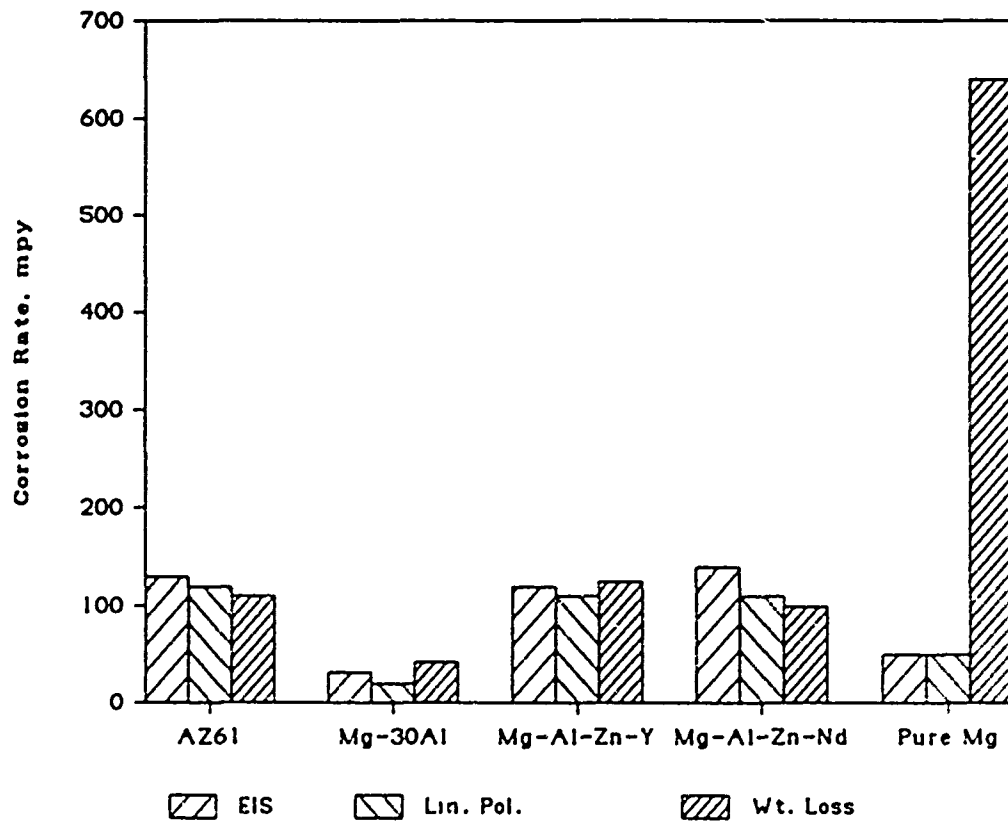


Figure 4



Figure 5



Figure 6



Figure 7

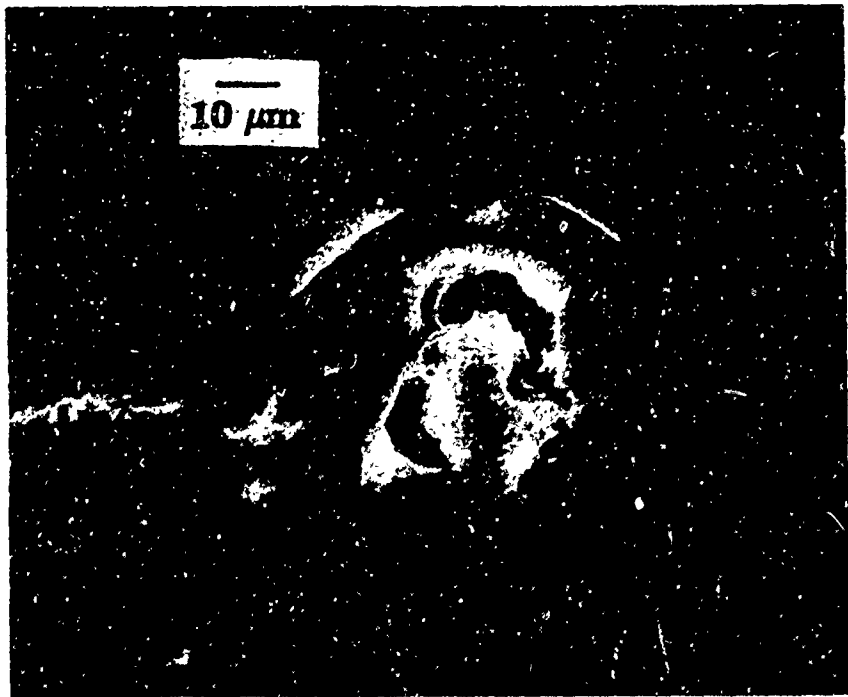


Figure 8

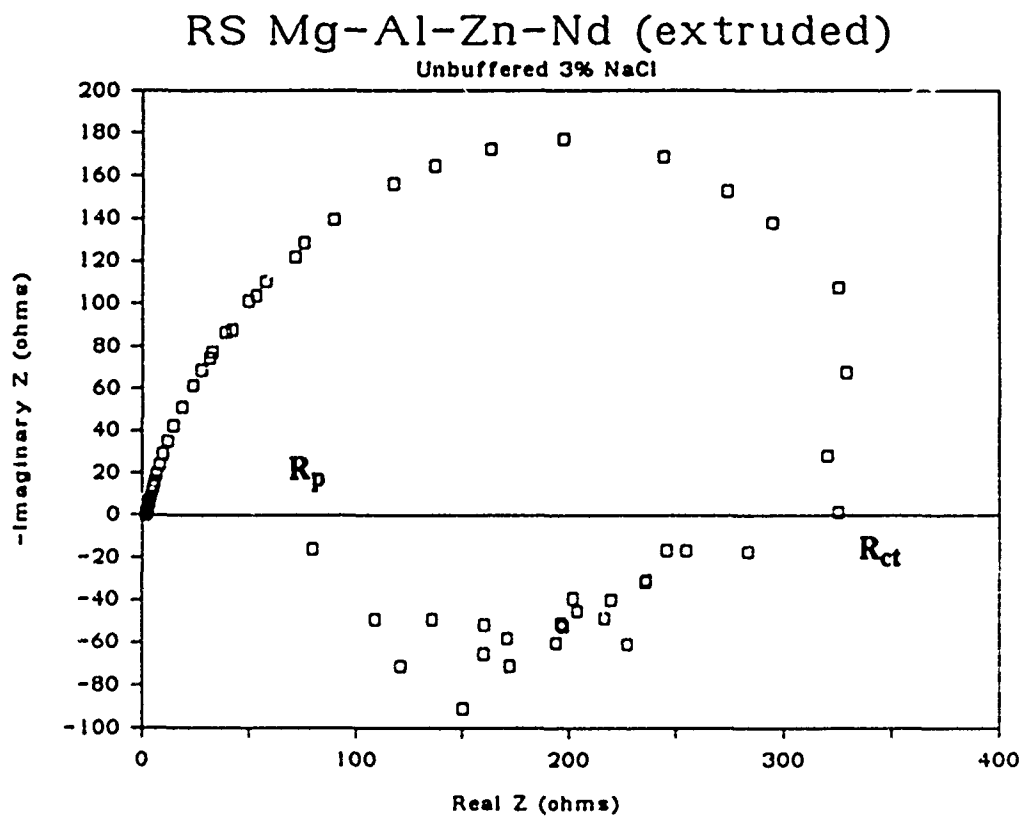


Figure 9

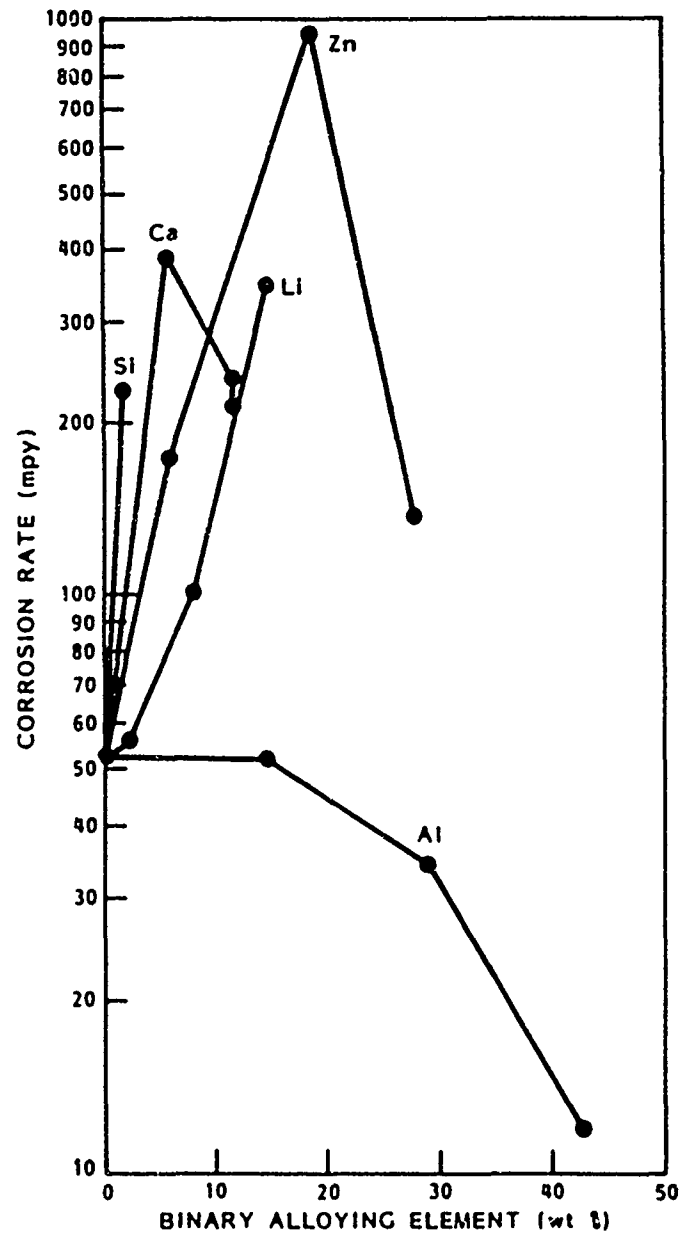


Figure 10

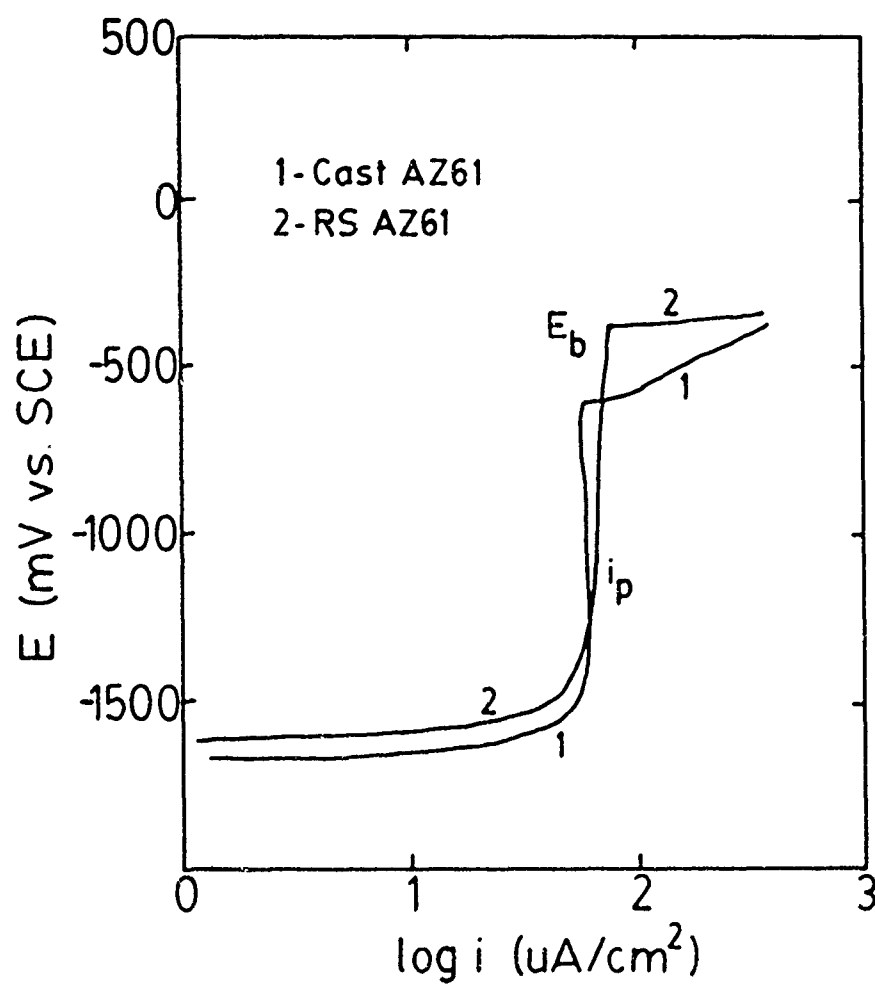


Figure 11

SECTION III

Structure of Surface Films

About 10 years ago, Revesz and Kruger [1] suggested that a noncrystalline structure is generally more desirable for a successful passive film than a crystalline structure. Of the many available (x-ray, neutron, and electron) scattering techniques, only x-ray absorption spectroscopy offers a direct surface-sensitive measurement of the (possibly) disordered structure of passive films on alloys. The challenge we undertook in such measurements was to study the passive film, which is often only of the order of a few nm thick, on the surface of a bulk metal or alloy containing many of the same elemental species. Two EXAFS techniques were available for such surface sensitive measurements. One was to employ partial yield electron detection, either in vacuum [2] or in the inert atmosphere of a photocathode detector [3], and the other was to follow the x-ray absorption through the use of surface reflectance measurements [4]. The latter technique is particularly suited for measurements on ultra-thin layers of oxide on low-Z (e.g. Mg) alloys because of the excellent signal-to-noise that accompanies the surface sensitivity at moderate reflection angles. The results reported in this work were derived from surface reflectance measurements of the thin films on magnesium and magnesium alloys in the neighborhood of the oxygen K-edge.

The Development of the ReflEXAFS Technique--The high reflectivity of x-rays at grazing incidence to a polished surface can be described using the Fresnel equations. These equations are derived from a consideration of plane waves incident on a planar boundary. Several conditions must be met for these assumptions to be valid: 1. the radius of curvature of the surface must be much greater than the wavelength of the light; 2. the reflecting medium is assumed to be homogeneous; and 3. the reflecting surface is assumed to be planar. The first condition is easily satisfied for x-rays. With regard to the second condition, even though the magnitude of the x-ray wavelengths is of the same order as the atoms, there is no experimental evidence that the reflecting medium does not behave as if it were homogeneous [5]. Because of the small surface area involved, pits and scratches in the surface detract little from the expected reflectivity. Microscopic roughness, however, can cause serious reflectivity problems.

The complex dielectric permeability is given by

$$\kappa = 1 - 2\delta - 2\beta i \quad (1)$$

The dielectric permeability determines the phase velocity of waves in the medium

$$v = \frac{c}{\sqrt{\kappa}}$$

and the complex refractive index is $n = \delta$. If both δ and β are much less than 1, then to first order

$$n = 1 - \delta - \beta i \quad (2)$$

In this approximation, $1 - \delta$ is related to the real part of the phase velocity of the wave in the medium and β is related to the absorption that we wish to measure. δ , which is called the unit decrement, is of the order of 10^{-5} - 10^{-6} for hard (~ 0.1 nm) x-rays, but is closer to 10^{-2} - 10^{-3} for the softer (~ 2.5 nm) x-rays relevant to this work. This means that second order corrections involving δ may be significant in soft-x-ray measurements. Generally, δ is always positive, so the refractive index for x-rays is less than 1. For a particular group of x-rays, the contribution to δ may be negative, as for wavelengths close to an absorption edge. Usually, however, the contributions to δ from other groups of electrons are positive so that the overall δ is still positive.

The critical angle for total reflection is defined in terms of δ as $\phi_c = \sqrt{2\delta}$. Although the reflectance is not actually equal to 1 at angles smaller than this, it can be quite high for reflectors that have negligible absorption. The behavior of the reflectance as a function of normalized glancing angle is shown for values of β/δ between zero and 1 in Fig. 1. For small values of β/δ , the value of the critical angle is defined. If the inflection point of the reflectance curve is chosen for the value of the critical angle, then we note that for β/δ larger than 0.63 the reflectance curves do not display an inflection point. The reflectance, however, is still accurately predicted by the theory.

The ratio for the amplitude of the reflectance is given by

$$\text{Amplitude} = \frac{E_{\perp}}{E_{0\perp}} \quad (3)$$

where \perp indicates that the electric vector is perpendicular to the plane of incidence. If we set $\phi = a + bi$, then the reflectance we measure can be written

$$R = \frac{(\phi - a)^2 + b^2}{(\phi + a)^2 + b^2}$$

where

$$a^2 = \frac{1}{2} \left\{ \sqrt{(\phi^2 - 2\delta)^2 + 4\beta^2} + (\phi^2 - 2\delta) \right\},$$

$$b^2 = \frac{1}{2} \left\{ \sqrt{(\phi^2 - 2\delta)^2 + 4\beta^2} - (\phi^2 - 2\delta) \right\}.$$

For the present study, the values of δ and β , both of which carry EXAFS information, are calculated for magnesium-oxide using equations that are valid close to the K-edge of oxygen [6,7].

Under "total" reflection conditions, there is no wave propagating into the medium. Instead, there are waves of varying amplitude (evanescent waves) present which decrease with increasing penetration. These waves enter the medium and then emerge again from the same surface. The $1/e$ penetration depth, d , can be calculated from the imaginary part of the reflectance (b) using

$$d = \frac{\lambda}{4\pi b}$$

where λ is the wavelength of the radiation.

Fig. 2 shows the penetration depth in MgO as a function of angle for a range of energies relevant to studies near the oxygen K-edge, where, for the purposes of calculation, the effects on λ are assumed to be dominated by oxygen 1s electrons. For angles less than approximately 2.3° , the penetration depth for all photon energies up to 800 eV is less than 3.0 nm.

Outside the region for "total" reflection, interference can take place for a thin film on the surface of a substrate. The periodicity of the interference pattern can be used to measure the thickness of such films if they are uniform.

Since the wavelengths of x-rays are about 100 times smaller than those of visible light, there is an increased concern about the smoothness of the reflecting surface. Since the glancing angle for x-rays is about 100 times smaller than for optical, the quality of the reflecting surface should be of the order of 20 times better.

Experimental Aspects (see 2nd Annual Report for more details)--Specimens of pure Mg, AZ61 Mg alloy, Mg15%Al, Mg30%Al, an Mg-Al-Zn-Nd alloy from Allied Signal Corp. that was extruded from crushed RS ribbons into bar form, and single crystals of MgO and Mg(OH)₂ that were used as standards were polished to a mirror-like finish. Films were formed on the Mg and Mg alloy surfaces by exposure to a humid atmosphere at 100c and to a borate buffer solution.

The surface reflectance measurements were performed on the U-15 beamline (SUNY/NSLS) at the National Synchrotron Light Source at Brookhaven National Laboratory. The beamline is equipped with a toroidal grating monochromator

(TGM) with a 600 line/mm gold coated grating. The TGM has a constant wavelength resolution which depends on the size of the aperture in front of the grating and on the electron beam in the storage ring.

The geometry of the reflEXAFS experiment is shown in Fig. 3. The soft x-rays entering the sample area impinge first on a gold mesh. The remainder of the beam impinges at grazing ($0.5^\circ < \theta < 3.5^\circ$) incidence on the sample and the reflected beam is measured.

A major problem in carrying out reflEXAFS measurements is the treatment of the data to remove the instrumental factors from the raw data. A considerable amount of time was spent during the past two years in the development of the methodology to do this. The spectral range for the measurements is from 480-1000 eV. A measure of the window transmission function over this range is provided by scans performed without the specimen in the beam. Next, corrections for the harmonic content in the beam intensities with and without the specimen in the beam, taking into consideration the second order reflectivity contributions. This treatment yields the EXAFS contributions that provide data on nearest neighbor distances, coordination numbers and degree of order for the Mg and O atoms in the films on the metal surface that control corrosion.

Structure of Films--ReflexAFS provides the following kinds of structural information: 1) the nearest neighbor distances (e.g. for the first shell the O-Mg distance, r_1), 2) the coordination number, n_1 , (for the first shell), and 3) the Debye-Waller factor, σ^2 , a measure of the degree of disorder. The results obtained for pure Mg and a number of alloys and the two standards, MgO and Mg(OH)₂, are given in Table I. They show that there are clearly two types of surface film structures involved. The first group, represented by pure Mg and AZ61, have films whose structures and compositions are close to MgO. AZ61, however, has a lower coordination number, suggesting greater static disorder in the film. The second group, Mg15%Al, Mg30%Al, and an extruded RSP alloy obtained from Allied-Signal Corp., appear to have more Mg(OH)₂ content in their surface films as reflected in their having larger O-Mg distances. The greatest degree of disorder was observed for the film on the RSP alloy with the Mg15%Al alloy not far behind. These results were suggested by the theoretical studies which tied degree of noncrystallinity to corrosion resistance.

TABLE I - RefLEXAFS Data

	r_1	n_1	σ_1
MgO	2.106	6.0	
Mg(OH) ₂	2.173	3.0	
Pure Mg	2.09	2.9	0.0054
AZ61	2.09	2.3	0.0056
Mg(15%)Al	2.12	3.1	0.0134
Mg(30%)Al	2.12	2.8	0.0056
RSP Mg Alloy	2.14	1.3	0.0112

List of Figures

- Figure 1 - The reflectance, R , as a function of the normalized glancing angle, ϕ/ϕ_c , for different values of β/δ .
- Figure 2 - Penetration depth in MgO as a function of grazing angle, ϕ , for a range of energies.
- Figure 3 - Geometry of the reflEXAFS surface reflectivity measurements.

References

1. A.G. Revesz and J. Kruger, in Passivity of Metals, R.P. Frankenthal and J. Kruger, Eds., The Electrochemical Society, Princeton, N.J. (1978) 137.
2. J. Stohr, D. Denley, and P. Persetti, *Phys. Rev. B.*, **18** (1978) 4132.
3. G.G. Long, J. Kruger, D.R. Black, and M. Kuriyama, *J. Electroanal. Chem.*, **150** (1983) 603.
4. R. Barchewitz, M. Cremonese-Visicato and G. Onori, *J. Phys. C: Sol. St. Phys.* **11** (1978) 4439.
5. V. Rehn in Low Energy X-Ray Diagnostics, D.T. Attwood and B.L. Henke, Eds., AIP Conf. Proc. No. 75, A.I.P., New York (1981) 162.
6. A.H. Compton and S.K. Allison, X-Rays in Theory and Experiment, 2nd Ed., Van Nostrand, Princeton, N.J. (1935) Chap. 4.
7. M.A. Blokhin, The Physics of X-Rays, 2nd Ed., State Publishing House of Technical-Theoretical Literature, Moscow (1957) Chap. 5.

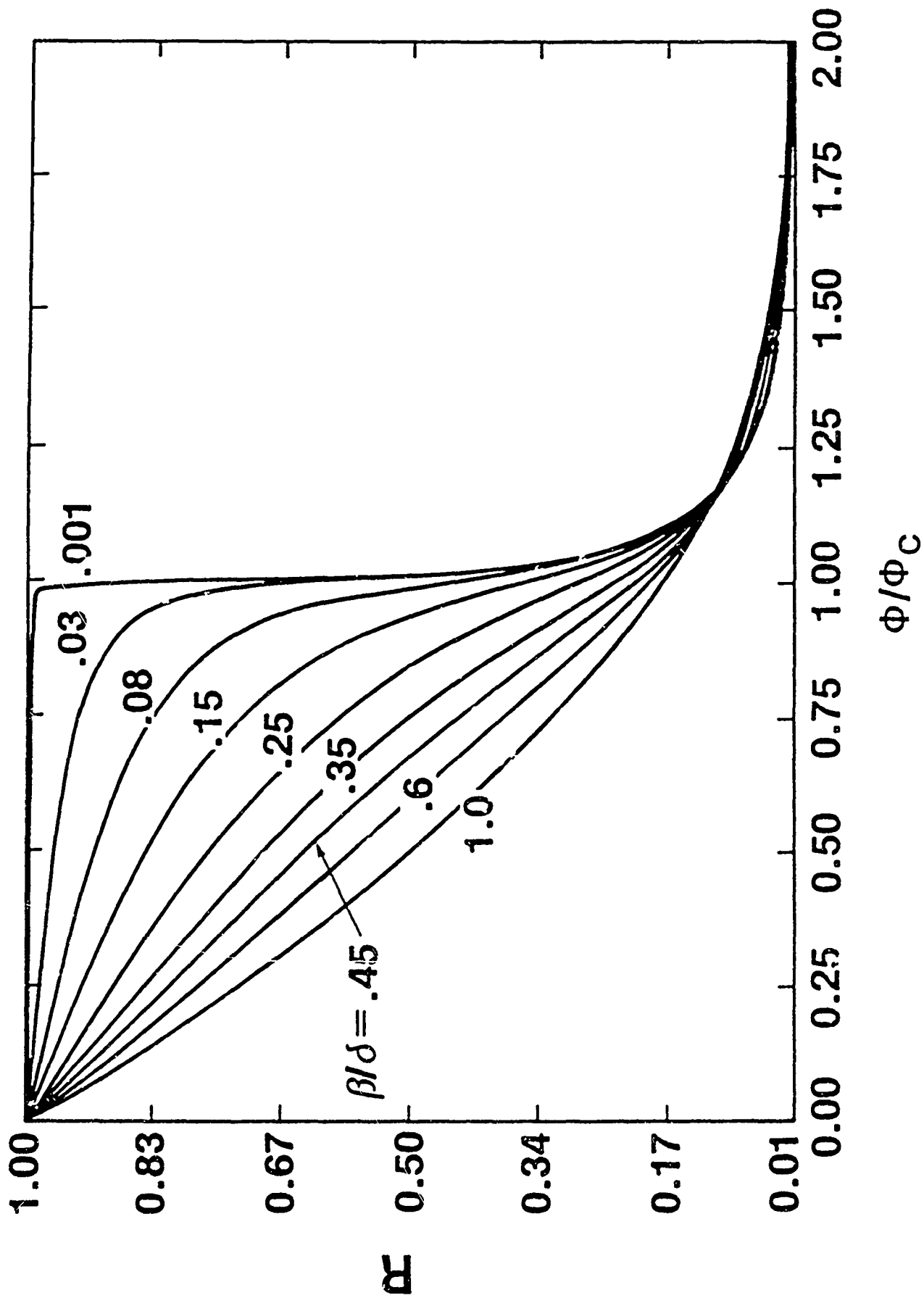


Figure 1

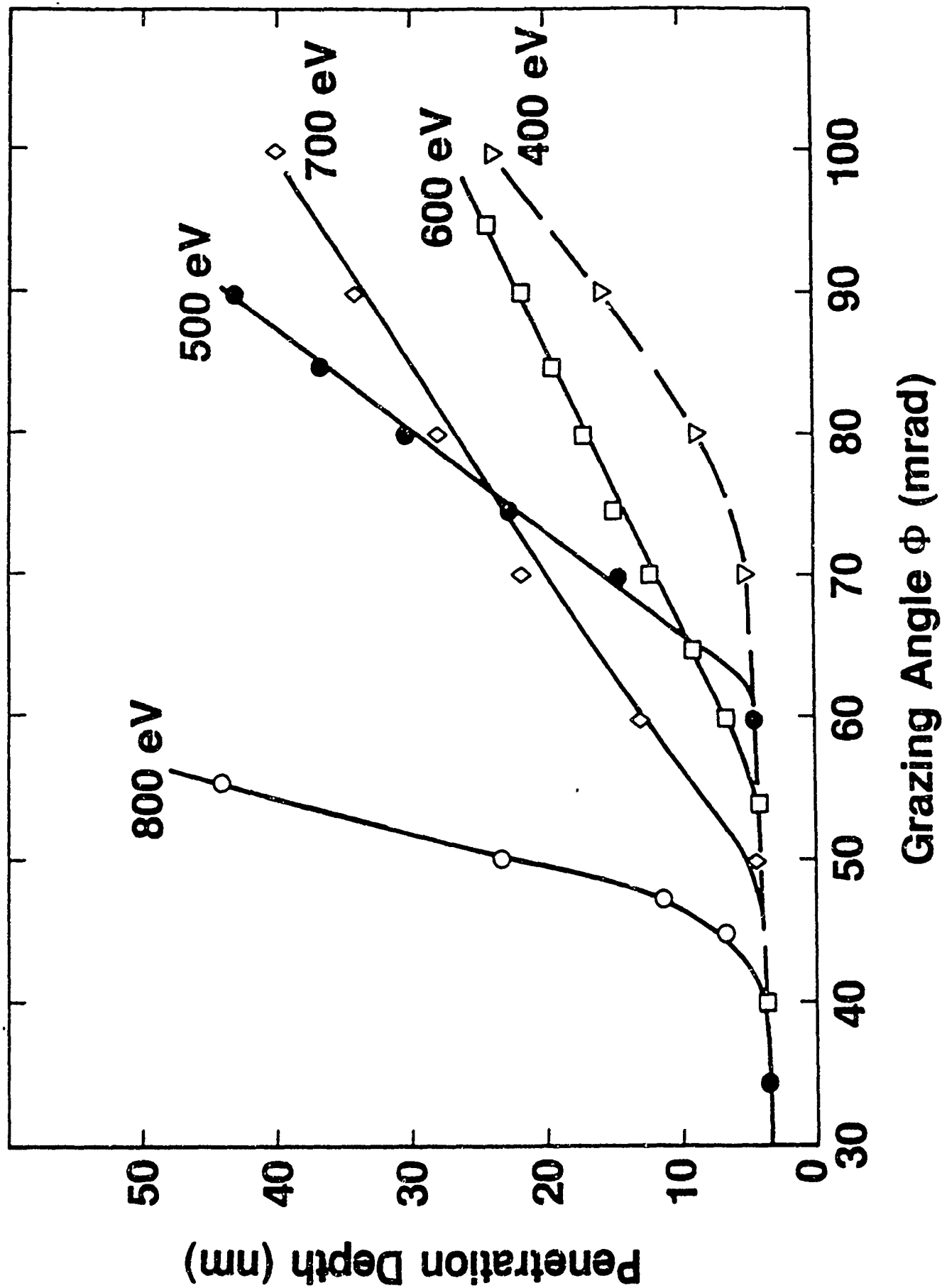


Figure 2

refLEXAFS Geometry

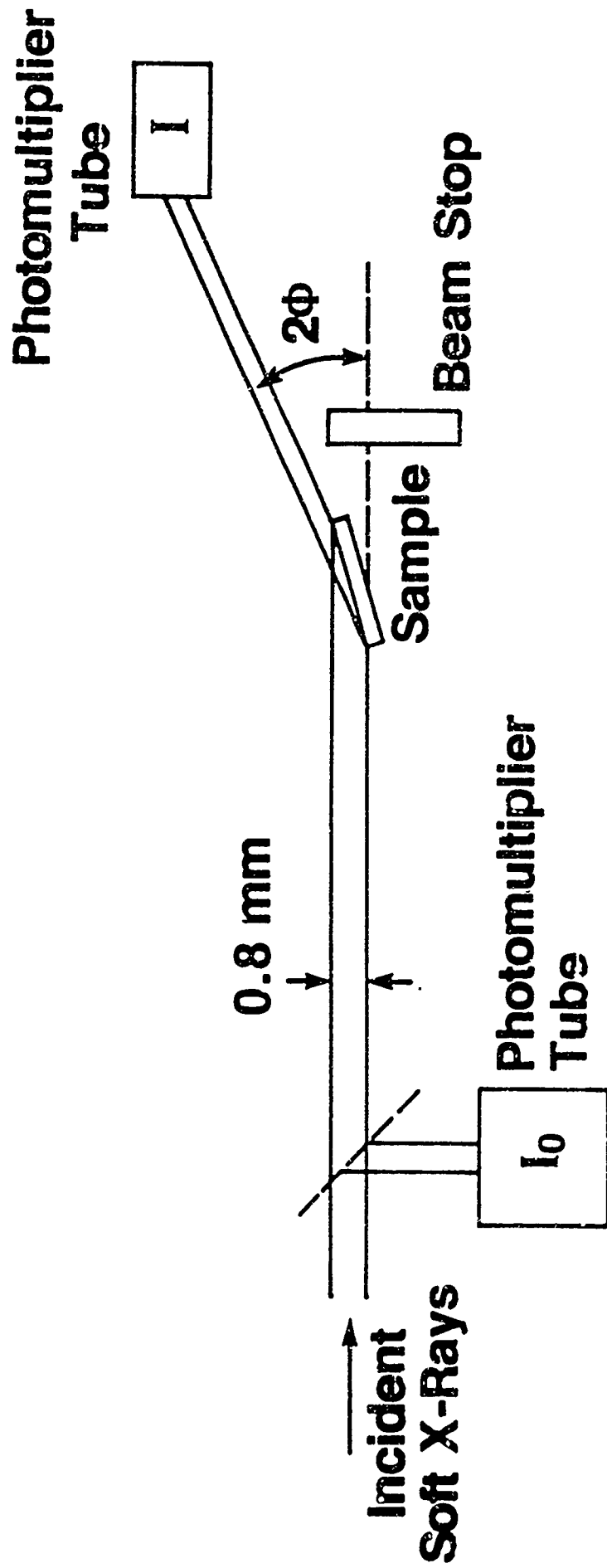


Figure 3

SECTION IV

Surface Analytical Studies of RSP Mg Alloys

Selected Mg-Zn and Mg-Al binary alloys and a Mg-Al-Li-Zn-Mn-Ce multi-component alloy were examined by Auger Electron Spectroscopy (AES) and X-ray Photoelectron Spectroscopy (XPS). Surface films on both sides of the ribbons and their modifications due to chemical treatments including exposure to sodium borate electrolyte were determined. Chemical treatments resulted in major changes in surface chemistry and surface film thickness which explain the differences in corrosion behavior. Experiments are continuing to fully understand these surface modifications and the precise mechanisms of corrosion. Some of the key observations (see Table I) are summarized below:

1. Surface oxides of most RS ribbons contain oxides of magnesium. Only lithium and calcium (among the alloys examined) have the tendency to be enriched in the oxide. The thickness and composition of the surface oxides vary with the bulk composition and with the cooling rate achieved during solidification. Carbonates and hydroxides were present at some of the examined surfaces and their role in corrosion needs to be understood.

2. Mg-Zn alloys exhibited differences in corrosion rates between the two sides of the RS ribbons, as a function of the bulk composition and as a function of the exposure time to the sodium borate electrolyte. Many of these differences can be explained by the surface chemical changes as determined by AES and XPS (see Table I). Typically, longer exposure times and glycol etch cause formation of relatively thick films in the 2000-7000 Å range and with substantial enrichment of zinc near the surface region. In contrast, surface oxides of ribbons in the as-RS condition are deficient in zinc and are only 100-200 Å in thickness.

TABLE I . SUMMARY OF SURFACE COMPOSITIONS OF MAGNESIUM ALLOYS
DETERMINED BY XPS

ALLOY	SURFACE*	CONDITION	SURFACE COMPOSITION (At.%)				
			Mg	Al	C	O	Other
Mg-14.4Al	FS	as RS	12.2	1.8	60.0	24.4	1.4 Si
		50Å Spu.	36.5	4.7	25.3	33.5	-
	WCS	as RS	11.4	1.7	67.0	18.6	1.3 Si
		50Å Spu.	33.5	4.7	31.4	28.3	2 Si
	WCS	etched**	3.3	1.9	71.1	22.7	1 Si
		etched + 50Å Spu.	8.6	4.7	62.9	23.9	-
Alloy 15	FS	as RS	6.3	1.4	31.0	40.0	21 Li
	WCS	as RS	6.5	0.8	33.0	42.0	17 Li
		as RS + expos. sod. Borate	12.2	4.0	24.5	47.9	8 B, 4 F, 0.1 Ce
		etched**	17.8	3.0	13.8	51.4	1 Zn, 13 P
	WCS	etched + expos. sod. Borate	47.0	5.3		42.3	5 B, 0.3 Ce

* Ribbon surfaces: FS - free surface
WCS - wheel contact surface

** Specimen was etched for 15 s using glycol etch.

SECTION V

Films and Stress Corrosion Cracking

The susceptibility of a material to initiation and propagation of stress corrosion cracks depends in part on how resistant its surface film is to breakdown, or in the event that breakdown occurs, how quickly and completely the film is repaired. Any explanation of stress corrosion cracking (SCC), also termed environment assisted cracking (EAC), requires an understanding of the breakdown/repassivation processes occurring on the surface of the metal or alloy being investigated. One important aspect of this phenomenon is the repassivation rate for a passive film which has suffered breakdown, and some experiments conducted to examine the repassivation kinetics for as-cast and rapidly solidified alloy AZ61 are described below. This study, initiated in the third year, seeks to examine the interrelationship between film breakdown (studied by the constant extension rate technique (CERT) and film repair or repassivation. The apparatus for applying CERT to RSP ribbons was designed and built during the past year and is shown in Figure 1. Also pictured in Figure 1 is a more detailed view of the gripping arrangement for the RS ribbons. This consists of a nylon block, about one inch square, which is connected by a rod to the load train. The block has a removable piece, allowing the ribbon to be placed inside and held firmly by the screws. For controlling electrochemical conditions, an electrical connection can be made through one of the screws, thus making the ribbon an electrode.

Experimental

Alloy AZ61 is a commercial alloy containing roughly 6 wt.% aluminum and 0.7 wt.% zinc. Experiments were conducted in 4 wt.% (0.21M) potassium chromate with 0.1 wt.% (0.0017M) sodium chloride, similar to the electrolytes employed in previous EAC studies of magnesium and Mg alloys [eg. 1,2]. The pH of this solution was 9.1. Both cast and RS ribbon samples were mounted in a room-temperature potting compound leaving a flat surface exposed; ribbon samples were mounted with the non-contact surface exposed. The surface of the cast alloy was polished to 600-grit SiC, rinsed in millipore water, then methanol, and finally dried in a stream of warm air before immersion. The RS samples were dipped for about 5 sec. in dilute HNO₃, then rinsed in millipore water, methanol, and dried in warm air.

After a stable open-circuit potential value was reached (usually about 2 hours), the potential was stepped to a value in the passive region (-750 mV vs. SCE), which was determined from polarization curves generated at 0.2 mV/s. After the current stabilized at this potential, a strip-chart recorder was used to monitor the current. To break down the film, the potential was stepped to +1 V vs. SCE for 5 sec., then returned to -750 mV. The subsequent current decay was recorded as a function of time. This procedure was carried out on both the freshly prepared surface and again after the surface repassivated.

Results

The polarization scans for the cast and RS material are presented in Figure 2. Note that the open-circuit potential (E_{oc}) for the RS material was highly reproducible, while that for the cast AZ61 varied from test to test between about -1.4 V and -1 V. While undergoing anodic polarization, both materials began to form a thick, black film at about -900 mV. The current density became stable at approximately $200 \mu\text{A}/\text{cm}^2$, and breakdown occurred at -300 mV for both materials.

Figure 3 shows the typical transients observed for the cast and RS AZ61 with both current density and time plotted on log scales. The behavior is approximately linear at the times observed. Beck has described such behavior in terms of a diffusion-limited current density as a salt film grows to fill the pit [3]. This current density was described by the following equation:

$$i_L = zFC_s \sqrt{\frac{D}{\pi t}} \quad (1)$$

where z is the number of electrons transferred per mole, F is Faraday's number, C_s is the saturation concentration of metal salt in the pit, D is the diffusion coefficient, and t is the time.

The slopes of the two lines shown in Figure 2 are nearly the same, indicating similar repassivation rates at these times. As the experimental technique is refined, it will be used to look more closely at the repassivation process, such as analyzing of the current behavior over a broader time frame. Another immediate goal is to determine more about the composition of the film, particularly the role of aluminum, as the future work will focus on RS Mg-Al binary alloys.

List of Figures

- Figure 1 - Schematic diagram of the apparatus for investigating stress corrosion cracking of RSP ribbons using the constant extension rate technique.
- Figure 2 - Anodic polarization scans for cast and RS AZ61 in 4 wt.% potassium chromate with 0.1 wt.% sodium chloride.
- Figure 3 - Log current vs. log time relationships for cast and RS AZ61 pulsed with a high anodic potential (+1V SCE) in 4 wt.% potassium chromate with 0.1 wt.% sodium chloride.

References

1. G. Oryall and D. Tromans, "Transgranular Stress Corrosion Cracking of Solution Treated and Quenched Mg-8.6Al Alloy," *Corrosion*, 27 (8) (1971), 334-341.
2. D.G. Chakrapani and E.N. Pugh, "Hydrogen Embrittlement in a Mg-Al Alloy," *Metallurgical Trans. A*, 7A (1976), 173-178.
3. T. Beck, "Fundamental Investigation of Pitting Corrosion in Structural Metals," Final Report to Office of Naval Research, July 1981, 11-14.

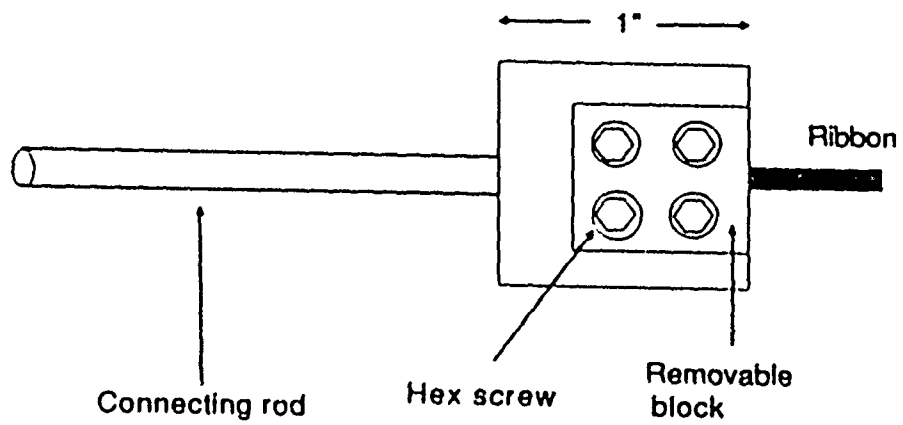
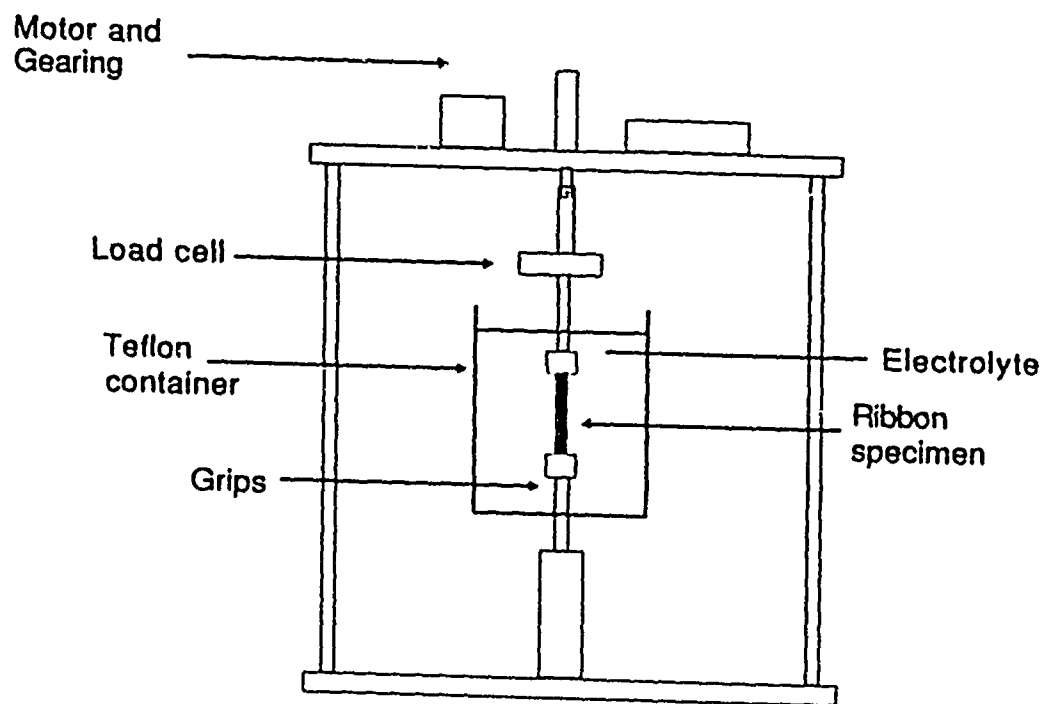


Figure 1

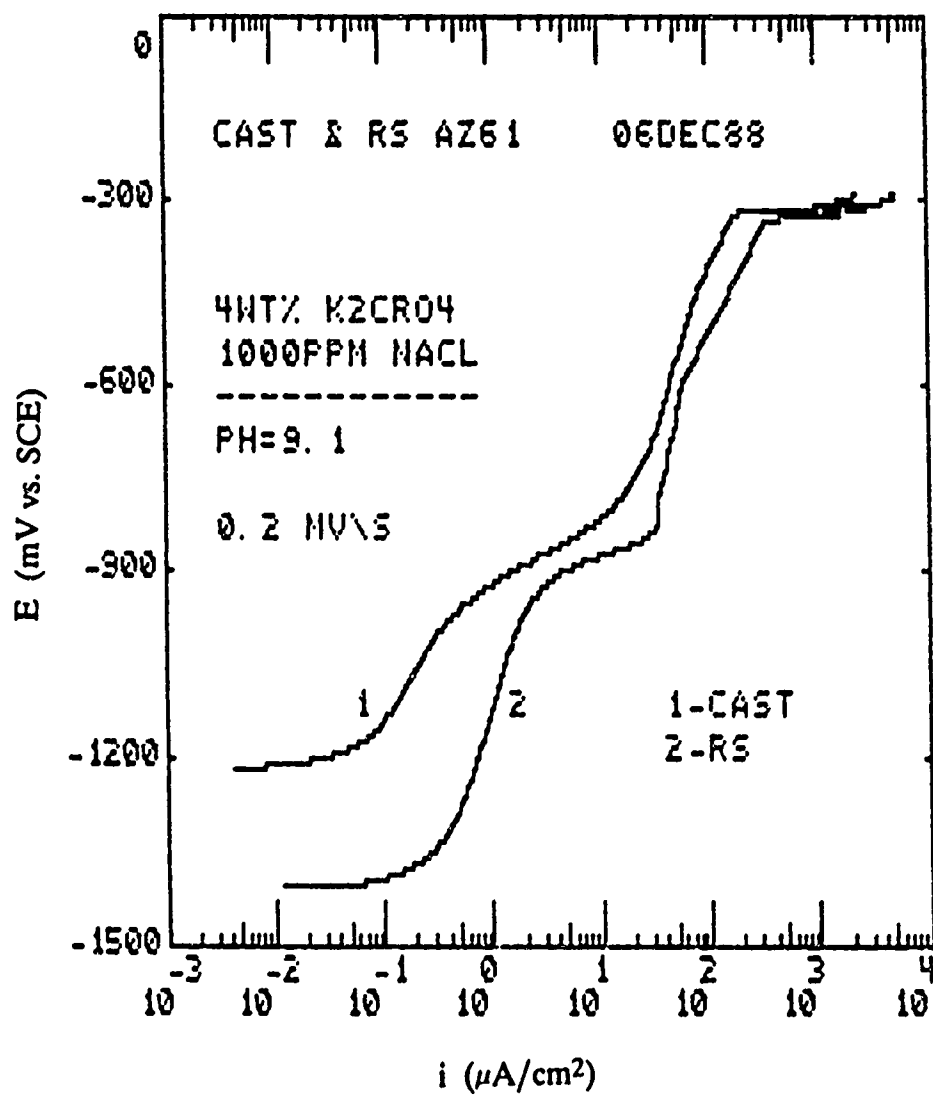


Figure 2

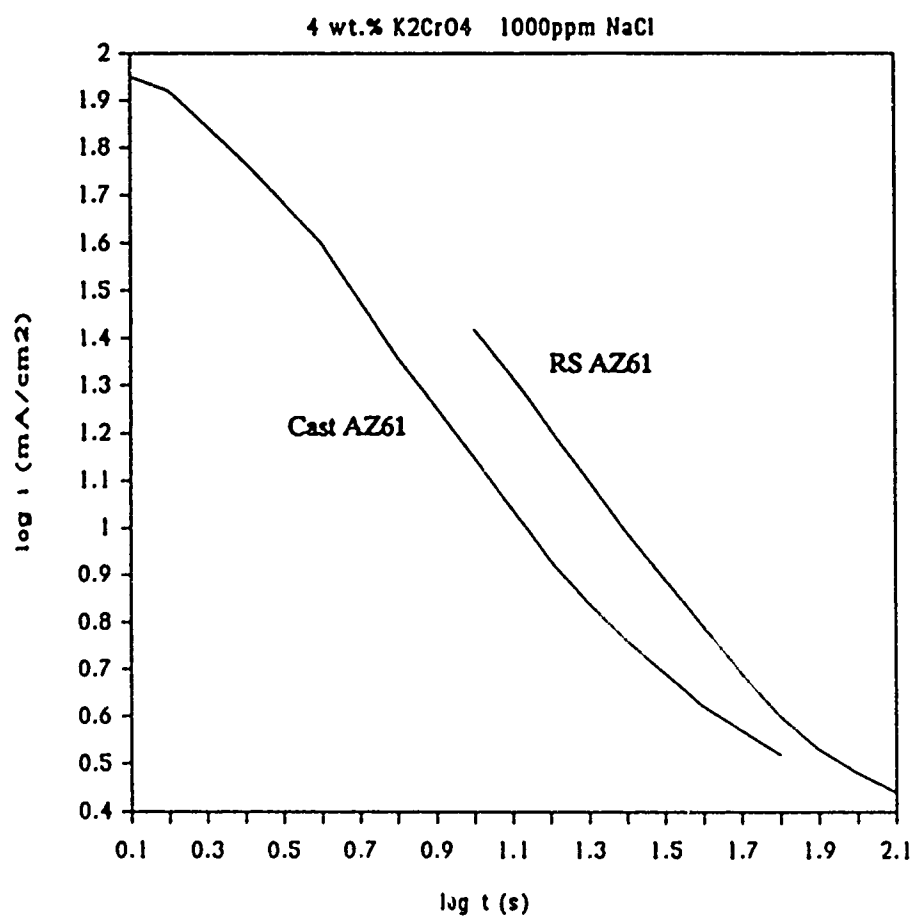


Figure 3